

Theory of Transport through Quantum-Dot Spin Valves in the Weak-Coupling Regime

Matthias Braun,^{1,2} Jürgen König,^{1,2} and Jan Martinek^{2,3,4}

¹*Institut für Theoretische Physik III, Ruhr-Universität Bochum, 44780 Bochum, Germany*

²*Institut für Theoretische Festkörperphysik, Universität Karlsruhe, 76128 Karlsruhe, Germany*

³*Institute for Materials Research, Tohoku University, Sendai 980-8577, Japan*

⁴*Institute of Molecular Physics, Polish Academy of Science, 60-179 Poznań, Poland*

(Dated: March 14, 2022)

We develop a theory of electron transport through quantum dots that are weakly coupled to ferromagnetic leads. The theory covers both the linear and nonlinear transport regime, takes non-collinear magnetization of the leads into account, and allows for an externally applied magnetic field. We derive generalized rate equations for the dot's occupation and accumulated spin and discuss the influence of the dot's spin on the transmission. A negative differential conductance and a nontrivial dependence of the conductance on the angle between the lead magnetizations are predicted.

PACS numbers: 72.25.Mk, 73.63.Kv, 85.75.-d, 73.23.Hk

I. INTRODUCTION

The study of spin-dependent transport phenomena has recently attracted much interest and led to new device functionalities based on the manipulation of the spin degree of freedom.^{1,2} A prominent example, which has already proven technological relevance, is the spin valve based on either the giant magnetoresistance effect³ in magnetic multilayers or the tunnel magnetoresistance⁴ in magnetic tunnel junctions. In the latter case, the tunneling current between two ferromagnets depends on the relative orientation of the leads' magnetizations. The maximal and minimal transmission is achieved for the parallel and antiparallel configurations, respectively. At intermediate angles ϕ of the relative magnetization direction, the transmission is interpolated by a cosine law. This angular dependence, which has been beautifully demonstrated experimentally,⁵ can be easily understood within a noninteracting-electron picture.⁶ It simply reflects the ϕ -dependent overlap of the spinor part of the majority-spin-electron wave functions in the source and drain electrodes.

On the other hand, tunneling transport through nanostructures, such as semiconductor quantum dots or metallic single-electron transistors, is strongly affected by Coulomb interaction, and a noninteracting-electron picture is no longer applicable. Recent works on spin-dependent tunneling through these devices include studies on metallic islands,^{7,8} granular systems,⁹ and carbon nanotubes¹⁰ coupled to ferromagnetic leads as well as spin-polarized transport from ferromagnets through quantum dots.^{11,12,13,14,15,16,17,18,19} The focus of this paper is on quantum-dot spin valves, i.e., quantum dots attached to ferromagnetic leads, with non-collinear magnetizations, see Fig. 1.

The much richer transport behavior of quantum-dot spin valves, as compared to single magnetic tunnel junctions, relies on the possibility to generate a non-equilibrium spin accumulation on the quantum dot, depending on system parameters such as gate and bias voltage, charging energy, asymmetry of the tunnel couplings,

and external magnetic field. This opens the potential of a controlled manipulation of the quantum-dot spin, detectable in transport. To some degree, there is a relation between the system under consideration and a single magnetic-atom spin on a scanning tunneling microscope tip. For the latter, precession of the single spin in an external magnetic field has been detected in the power spectrum of the tunneling current.^{20,21}

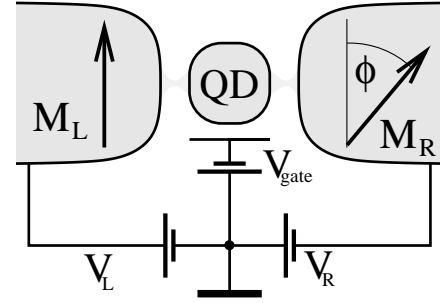


FIG. 1: Quantum-dot spin valve: a quantum dot is weakly coupled to ferromagnetic leads. The magnetization directions of the leads enclose an angle ϕ .

In a recent Letter by two of us,¹¹ we predicted that the interplay of spin-dependent tunneling and Coulomb interaction in quantum-dot spin valves gives rise to an interaction-driven spin precession, describable in terms of an exchange field and detectable in a nontrivial ϕ dependence of the linear conductance. The aim of the present paper is to extend this discussion to a complete theory of transport through quantum-dot spin valves in the limit of weak dot-lead coupling.²² The theory covers both the regimes of linear and nonlinear response, and is easily generalized to include an external magnetic field and/or spin relaxation processes within the quantum dot. The quantities of central interest are the magnitude and direction of the spin accumulated on the quantum dot. They can be determined by generalized kinetic equations within a diagrammatic real-time transport theory for the dot's density matrix. To obtain a more intuitive and eas-

ily accessible framework for the dynamics of the dot's occupation and spin, however, we transform the kinetic equations into rate equations that exhibit similarities to Bloch equations of a spin in a magnetic field. The derivation of these Bloch-like rate equations is the first central result of this paper, presented in Sec. III after defining the model in Sec. II. They provide a convenient starting point for the discussion of how the dot state depends on the system parameters. The second major achievement of this paper is to relate the current through the device to the dot's occupation and average spin, which is done in Sec. IV.

An analysis of the obtained results is presented in Sec. V. We find that the quantum-dot spin, and thus the current, behaves quite differently in the linear- and nonlinear-response regime. In linear response, the above-mentioned effective exchange field rotates the quantum-dot spin such that the spin-valve effect is reduced. This contrasts with the nonlinear-response regime, in which the dot spin tends to align antiparallel to the drain electrode, leading to a spin blockade. Together with the effective exchange field this leads to a very pronounced negative differential conductance.

We, then, conclude by generalizing our theory to include an external magnetic field (Sec. VI) or internal spin relaxation in the dot (Sec. VII), and by interpreting the effective exchange field within the recently introduced²³ language of the spin-mixing conductance (Sec. VIII).

II. MODEL

We consider a quantum dot with a level spacing exceeding thermal broadening, intrinsic linewidth, and charging energy, i.e., only a single level with energy ε , measured relative to the Fermi energy of the leads, contributes to transport. The quantum dot is tunnel-coupled to ferromagnetic leads. We model this system with the Hamiltonian

$$H = H_{\text{dot}} + H_L + H_R + H_{T,L} + H_{T,R}. \quad (2.1)$$

The first part $H_{\text{dot}} = \sum_{\sigma} \varepsilon_{\sigma}^{\dagger} c_{\sigma} + U n_{\uparrow} n_{\downarrow}$ describes an atomiclike spin-degenerate energy level on the dot plus the charging energy U for double occupancy. The left and right ferromagnetic leads, $r = L, R$, are treated as a reservoir of itinerant electrons, $H_r = \sum_{k\sigma} \varepsilon_{k\sigma} a_{rk\sigma}^{\dagger} a_{rk\sigma}$, where $\sigma = +$ labels majority and $\sigma = -$ minority-spin electrons. Here, the quantization axis for the electron spins in reservoir r is chosen along its magnetization direction $\hat{\mathbf{n}}_r$. In the spirit of a Stoner model of ferromagnetism, we assume a strong spin asymmetry in the density of states $\rho_{r,\pm}(\omega)$ for majority (+) and minority (-) spins. (To be more precise, without loss of generality we assume the direction of magnetization to be parallel to the direction of majority spins.) In the following, the densities of states are approximated to be energy independent $\rho_{r,\pm}(\omega) = \rho_{r,\pm}$. (Real ferromagnets have a structured density of states. This will modify details of our results but not change the

general physical picture.) The asymmetry in the density of states is characterized by the degree of spin polarization $p_r = (\rho_{r+} - \rho_{r-})/(\rho_{r+} + \rho_{r-})$ with $0 \leq p_r \leq 1$, where $p_r = 0$ corresponds to a nonmagnetic lead, and $p_r = 1$ describes a half-metallic lead, carrying majority spins only. The magnetization directions of the leads can differ from each other, enclosing an angle $\phi = \angle(\hat{\mathbf{n}}_L, \hat{\mathbf{n}}_R)$. An applied bias voltage is accounted for in different electrochemical potentials for the left and right leads.

Tunneling between leads and dot is described by tunnel Hamiltonians $H_{T,L}$ and $H_{T,R}$. Their explicit form depends on the choice of the spin quantization axis for the dot states. We find it convenient to choose neither $\hat{\mathbf{n}}_L$ nor $\hat{\mathbf{n}}_R$ but instead to quantize the dot spin $\sigma = \uparrow, \downarrow$ along the z -direction of the coordinate system in which the basis vectors $\hat{\mathbf{e}}_x$, $\hat{\mathbf{e}}_y$, and $\hat{\mathbf{e}}_z$ are along $\hat{\mathbf{n}}_L + \hat{\mathbf{n}}_R$, $\hat{\mathbf{n}}_L - \hat{\mathbf{n}}_R$, and $\hat{\mathbf{n}}_R \times \hat{\mathbf{n}}_L$, respectively (see also Fig. 2). The tunnel

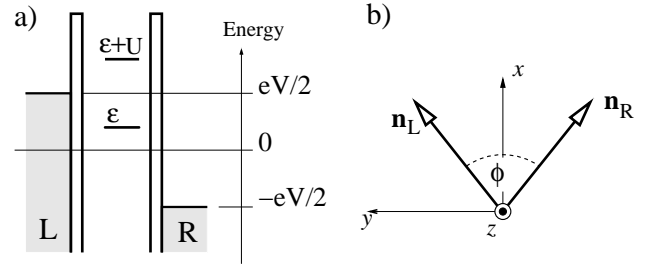


FIG. 2: (a) Scheme of the quantum-dot energy scales. The difference of the electrochemical potentials of the left and right leads describes a symmetrically applied bias voltage. (b) The coordinate system we choose. The magnetization directions $\hat{\mathbf{n}}_L$ and $\hat{\mathbf{n}}_R$ enclose an angle ϕ .

Hamiltonian for the left tunneling barrier then reads

$$H_{T,L} = \frac{t_L}{\sqrt{2}} \sum_k a_{Lk+}^{\dagger} (e^{+i\phi/4} c_{\uparrow} + e^{-i\phi/4} c_{\downarrow}) + a_{Lk-}^{\dagger} (-e^{+i\phi/4} c_{\uparrow} + e^{-i\phi/4} c_{\downarrow}) + \text{H.c.} \quad (2.2)$$

and for the right barrier, $H_{T,R}$, the same with the replacements $L \rightarrow R$ and $\phi \rightarrow -\phi$. Here, t_L and t_R are the tunnel matrix elements. The tunneling rate for electrons from lead r with spin (\pm) is then $\Gamma_{r,\pm}/\hbar = 2\pi|t_r|^2 \rho_{r,\pm}/\hbar$. Therefore the electronic states in the quantum dot with spin ($\uparrow\downarrow$) acquire a finite line width $\Gamma_r = \sum_{\sigma=\pm} 2\pi|t_r/\sqrt{2}|^2 \rho_{r,\sigma} = \sum_{\sigma=\pm} \Gamma_{r,\sigma}/2$.

We note that while individual parts of the tunnel Hamiltonians do not conserve spin separately, the sum of all parts strictly does. Due to the special choice of the quantization axis, the lead electrons are coupled equally strong to up- and down-spin states in the quantum dot. There are, however, phase factors involved, similar to Aharonov-Bohm phases in multiply connected geometries. The formal similarity of the quantum-dot spin valve to a two-dot Aharonov-Bohm interferometer²⁴ is visualized in Fig. 3.

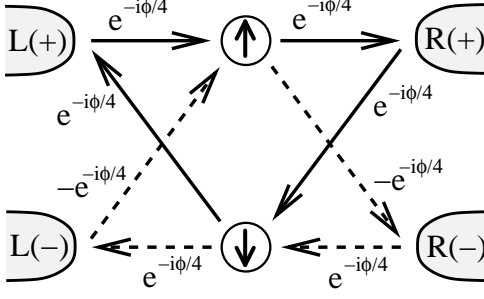


FIG. 3: Graphical representation of the phase factors in the tunnel Hamiltonian, Eq. (2.2). In this representation, the quantum-dot spin valve bears similarities to an Aharonov-Bohm setup, with the different spin channels \uparrow and \downarrow , and the Aharonov-Bohm flux corresponding to the relative angle of the leads' magnetizations.

III. OCCUPATION AND SPIN OF THE DOT

In this section we derive rate equations governing the state of the dot, i.e., its occupation as well as the magnitude and direction of an accumulated spin. For this, we make use of a diagrammatic real-time approach²⁵ to describe the time evolution of the reduced density matrix for the dot degree of freedoms, which is obtained after integrating out the lead electrons. The resulting equations for the density matrix elements can be reformulated into a more intuitive language of rate equations for the dot's occupation and spin.

A. Reduced density matrix for the quantum dot

The dynamics of the system can be described by the time evolution of the total density matrix, which accounts for all degrees of freedom in the dot and the leads. While the leads are treated as reservoirs of noninteracting electrons, it is the dynamics of the dot degrees of freedom that determine the transport behavior. This motivates the idea to integrate out the leads and arrive at a reduced density matrix for the dot degrees of freedom only. Details about the procedure of integrating out the leads are given in Ref. 25.

The basis of the Hilbert space is given by the states $\chi = 0$ (empty dot), \uparrow (dot occupied with one spin-up electron), \downarrow (the same with a spin-down electron), and d (double occupancy of the dot). Therefore, the reduced density matrix ρ_{dot} is a 4×4 matrix with matrix elements $P_{\chi_2}^{\chi_1} \equiv (\rho_{\text{dot}})_{\chi_1 \chi_2}$. We get

$$\rho_{\text{dot}} = \begin{pmatrix} P_0 & 0 & 0 & 0 \\ 0 & P_{\uparrow} & P_{\uparrow}^{\downarrow} & 0 \\ 0 & P_{\downarrow}^{\uparrow} & P_{\downarrow} & 0 \\ 0 & 0 & 0 & P_d \end{pmatrix}. \quad (3.1)$$

The diagonal, real entries $P_{\chi} \equiv P_{\chi}^{\chi}$ are nothing but the probabilities to find the dot in the corresponding state $\chi = 0, \uparrow, \downarrow, d$. The zeros in Eq. (3.1) in the off diagonals are a consequence of the total-particle-number conservation. The nonvanishing complex off-diagonal elements $P_{\downarrow}^{\uparrow} = (P_{\uparrow}^{\downarrow})^*$ reflect the fact that an accumulated dot spin is not restricted to the z direction but can also have a finite x and y component. The density matrix has, thus, six real parameters (four diagonal elements and the real and imaginary parts of $P_{\uparrow}^{\downarrow}$). Due to the normalization condition $\text{Tr } \rho_{\text{dot}} = 1$, only five of them are independent.

The time evolution of the reduced density matrix is given by a generalized master equation in Liouville space²⁵,

$$\begin{aligned} \frac{d}{dt} P_{\chi_2}^{\chi_1}(t) &= -\frac{i}{\hbar} (E_{\chi_1} - E_{\chi_2}) P_{\chi_2}^{\chi_1}(t) \\ &+ \int_{-\infty}^t dt' \sum_{\chi_1' \chi_2'} P_{\chi_2'}^{\chi_1'}(t') \Sigma_{\chi_2' \chi_2}^{\chi_1' \chi_1}(t', t). \end{aligned} \quad (3.2)$$

Here, E_{χ_i} are the energies of the decoupled system (in our case $E_0 = 0$, $E_{\uparrow} = E_{\downarrow} = \varepsilon$, and $E_d = 2\varepsilon + U$). The kernels $\Sigma_{\chi_2' \chi_2}^{\chi_1' \chi_1}(t', t)$ act as generalized transition rates in Liouville space. They are defined as irreducible self-energy parts of the dot propagator on a Keldysh contour (see appendix A 1), and can be expanded in powers of the dot-lead coupling strength Γ . In the limit of interest for this paper, i.e., weak dot-lead coupling, only the terms linear in Γ are retained.

The Markovian approximation is established by replacing $P_{\chi_2'}^{\chi_1'}(t')$ in Eq. (3.2) with $P_{\chi_2'}^{\chi_1'}(t)$. In this case, the time integral can be comprised in the definition $\Sigma_{\chi_2' \chi_2}^{\chi_1' \chi_1} = i\hbar \int_{-\infty}^0 dt' \Sigma_{\chi_2' \chi_2}^{\chi_1' \chi_1}(t', 0)$. We will only discuss results for the steady-state limit, i.e., all matrix elements are time independent and the above-mentioned replacement is not an approximation but valid in general. In order to emphasize the physical origin of the rate equations, however, we will keep all time derivatives although their numerical value is zero for our discussion.

B. Master and Bloch-like equations

For a more intuitive access to the average dot state, we connect the matrix elements of the reduced density matrix to the vector of the average spin $\hbar \mathbf{S}$ with $\mathbf{S} = (S_x, S_y, S_z)$ by

$$S_x = \frac{P_{\downarrow}^{\uparrow} + P_{\uparrow}^{\downarrow}}{2}; \quad S_y = i \frac{P_{\downarrow}^{\uparrow} - P_{\uparrow}^{\downarrow}}{2}; \quad S_z = \frac{P_{\uparrow} - P_{\downarrow}}{2}. \quad (3.3)$$

We emphasize that the \mathbf{S} describes a quantum-statistical average rather than the coherent state of a single spin. As a consequence, the magnitude $|\mathbf{S}|$ can adopt any number between 0 and $1/2$. The average charge occupation of the dot is determined by the probabilities P_0 , P_1 , and

P_d , where $P_1 = P_\uparrow + P_\downarrow$. The dot state is, thus, characterized by the set of parameters $(P_0, P_1, P_d, S_x, S_y, S_z)$, in which only five of them are independent, since the normalization of the probabilities requires $P_0 + P_1 + P_d = 1$.

We evaluate the irreducible self-energies appearing in

$$\begin{aligned} \frac{d}{dt} \begin{pmatrix} P_0 \\ P_1 \\ P_d \end{pmatrix} &= \sum_{r=L,R} \frac{\Gamma_r}{\hbar} \begin{pmatrix} -2f_r^+(\varepsilon) & f_r^-(\varepsilon) & 0 \\ 2f_r^+(\varepsilon) & -f_r^-(\varepsilon) - f_r^+(\varepsilon + U) & 2f_r^-(\varepsilon + U) \\ 0 & f_r^+(\varepsilon + U) & -2f_r^-(\varepsilon + U) \end{pmatrix} \begin{pmatrix} P_0 \\ P_1 \\ P_d \end{pmatrix} \\ &+ \sum_{r=L,R} \frac{2p_r\Gamma_r}{\hbar} \begin{pmatrix} f_r^-(\varepsilon) \\ -f_r^-(\varepsilon) + f_r^+(\varepsilon + U) \\ -f_r^+(\varepsilon + U) \end{pmatrix} \mathbf{S} \cdot \hat{\mathbf{n}}_r. \end{aligned} \quad (3.4)$$

Here, we have used the following definitions. The probability to find an electronic state at energy ω in the left (right) lead occupied is given by the Fermi function $f_{L(R)}^+(\omega)$ and by $f_{L(R)}^-(\omega) = 1 - f_{L(R)}^+(\omega)$ to find it empty.

In the case of nonmagnetic leads, $p_r = 0$, only the first line in Eq. (3.4) survives, and we recover the usual master equations for sequential tunneling through a single level.²⁶ For spin-polarized leads, however, tunneling into or out of the dot becomes spin dependent. As a consequence, the charge occupation, in general, depends

Eq. (3.2) up to first order in Γ (see Appendix A) to get a set of six master equations, three for the occupation probabilities and three for the average spin. The first three are given by

on the spin \mathbf{S} accumulated on the dot, as indicated by the second line of Eq. (3.4). The three remaining master equations describe the time evolution of the average spin,

$$\frac{d\mathbf{S}}{dt} = \left(\frac{d\mathbf{S}}{dt} \right)_{\text{acc}} + \left(\frac{d\mathbf{S}}{dt} \right)_{\text{rel}} + \left(\frac{d\mathbf{S}}{dt} \right)_{\text{rot}} \quad (3.5)$$

with

$$\left(\frac{d\mathbf{S}}{dt} \right)_{\text{acc}} = \sum_{r=L,R} \frac{p_r\Gamma_r}{\hbar} \left[f_r^+(\varepsilon)P_0 + \frac{-f_r^-(\varepsilon) + f_r^+(\varepsilon + U)}{2}P_1 - f_r^-(\varepsilon + U)P_d \right] \hat{\mathbf{n}}_r \quad (3.6)$$

$$\left(\frac{d\mathbf{S}}{dt} \right)_{\text{rel}} = - \sum_{r=L,R} \frac{\Gamma_r}{\hbar} [f_r^-(\varepsilon) + f_r^+(\varepsilon + U)] \mathbf{S} \quad (3.7)$$

$$\left(\frac{d\mathbf{S}}{dt} \right)_{\text{rot}} = \mathbf{S} \times \sum_{r=L,R} \mathbf{B}_r, \quad (3.8)$$

where we used the definition

$$\mathbf{B}_r = p_r \frac{\Gamma_r \hat{\mathbf{n}}_r}{\pi \hbar} \int' d\omega \left(\frac{f_r^+(\omega)}{\omega - \varepsilon - U} + \frac{f_r^-(\omega)}{\omega - \varepsilon} \right) \quad (3.9)$$

for $r = L, R$, and the prime at the integral symbolizes Cauchy's principal value. We see that three different contributions lead to a change of the average dot spin. The first one, Eq. (3.6), depends on the occupation probabilities only and describes nonequilibrium spin accumulation via tunneling to and from spin-polarized leads. This is the source term, which is responsible for building up a spin polarization in the quantum dot. The second term (proportional to \mathbf{S}) has the opposite effect. It accounts for the decay of the dot spin by tunneling out of the electron with given spin or by tunneling in of a second elec-

tron with opposite spin forming a spin singlet on the dot. These tunneling mechanisms yield an intrinsic spin relaxation rate $1/\tau_c = \sum_{r=L,R} (\Gamma_r/\hbar) [f_r^-(\varepsilon) + f_r^+(\varepsilon + U)]$. From Eq. (3.5) we can derive the magnitude of the spin on the dot via

$$\frac{d|\mathbf{S}|}{dt} = \frac{\mathbf{S}}{|\mathbf{S}|} \cdot \left(\frac{d\mathbf{S}}{dt} \right)_{\text{acc}} - \frac{|\mathbf{S}|}{\tau_c}. \quad (3.10)$$

The two contributions, Eqs. (3.6) and (3.7), capture the spin dynamics due to spin-dependent tunneling processes transferring electrons into and out of the quantum dot. But above equation is also sensitive to the direction of \mathbf{S} , which depends directly on the third contribution, Eq. (3.8), of the Bloch-like equation. This term leads

to a precession of the dot spin about $\mathbf{B}_L + \mathbf{B}_R$, where $(\mathbf{B}_L + \mathbf{B}_R)/\gamma$ can be viewed as a fictitious magnetic field, with $\gamma = -g\mu_B$ being the gyromagnetic ratio. This fictitious field vanishes in the absence of Coulomb interaction, $U = 0$, i.e., its origin is a many-body interaction effect. Its nature can be conceived as an exchange field due to virtual particle exchange with the spin-polarized leads. Note that these virtual exchange processes do not change the charge of the dot, in contrast to the spin-dependent tunneling events responsible for the first two contributions to Eq. (3.5). Nevertheless, this contribution is also linear in Γ and has to be kept to be consistent. We emphasize that the use of a simple rate-equation picture, which neglects this exchange field and takes into account spin-dependent tunneling only, would be fundamentally insufficient.

The type of exchange interaction that emerges in our theory has been discussed in the literature in the context of Kondo physics for magnetic impurities in (normal) metals.²⁷ With the help of a Schrieffer-Wolff transformation, the Anderson Hamiltonian describing the magnetic impurity can be transformed to an s-d model, in which the spin of the magnetic impurity is coupled to the conduction-band-electron spins of the metal. Since the metal is spin symmetric, there is no net exchange field, though. This contrasts with our model, which includes a finite spin polarization of the leads. By integrating out the lead electrons of the transformed Hamiltonian in the subspace of single dot occupancy, we recover the precise mathematical form of the exchange field as given in Eq. (3.9).

The generalization of our theory to the case of real ferromagnets with nonuniform density of states is straightforward. The only modification is to keep the energy dependence of $p_r(\omega) \equiv [\rho_{r+}(\omega) - \rho_{r-}(\omega)]/[\rho_{r+}(\omega) + \rho_{r-}(\omega)]$ and $\Gamma_r(\omega)$ in all formulas. In particular, these quantities have to be included in the energy integral for the exchange field in Eq. (3.9).^{28,29}

We remark that the effective exchange field is not only responsible for the torque on an accumulated spin as discussed above, but it also generates a spin splitting of the dot level.³² Since this Zeeman-like splitting is proportional to Γ , it cannot be resolved in any transport signal in the weak-coupling regime considered in the present paper. This splitting gives rise to a correction of higher order in the coupling that has to be dropped in a consistent first-order-transport calculation. This contrasts with the limit of strong lead-dot coupling, in which any spin splitting modifies the emerging Kondo physics in a crucial manner.¹⁵

IV. ELECTRIC CURRENT

The current through the device can be expressed in terms of Keldysh Green's functions of electrons, as shown, e.g., in Refs. 24,30. The starting point of our discussion is the relation for the current I_r coming from

reservoir r ,

$$I_r = \frac{i(-e)}{\hbar} \int d\omega \operatorname{tr} \{ \Gamma_r f_r^+(\omega) \mathbf{G}^>(\omega) + \Gamma_r f_r^-(\omega) \mathbf{G}^<(\omega) \}. \quad (4.1)$$

Here, the bold face indicates a 2×2 matrix structure for the spin degree of freedom. The lesser and greater Green's functions $\mathbf{G}^<(\omega) = \begin{pmatrix} G_{\uparrow\uparrow}^<(\omega) & G_{\uparrow\downarrow}^<(\omega) \\ G_{\downarrow\uparrow}^<(\omega) & G_{\downarrow\downarrow}^<(\omega) \end{pmatrix}$ and $\mathbf{G}^>(\omega)$ are defined as the Fourier transforms of $G_{\sigma\sigma'}^<(t) = i\langle c_{\sigma'}^\dagger(0)c_\sigma(t) \rangle$ and $G_{\sigma\sigma'}^>(t) = -i\langle c_\sigma(t)c_{\sigma'}^\dagger(0) \rangle$, respectively. The coupling matrices are defined as $\Gamma_L = \begin{pmatrix} 1 & p_L e^{-i\phi/2} \\ p_L e^{+i\phi/2} & 1 \end{pmatrix}$, and the same for Γ_R but with the substitutions $L \rightarrow R$ and $\phi \rightarrow -\phi$. The diagonal matrix elements describe tunneling of spins along the z direction and are, therefore, independent of the leads' spin polarization p_r since the magnetizations of the leads lie in the $x-y$ plane. This contrasts with the off-diagonal matrix elements taking into account tunneling of spins in the $x-y$ plane.

In the weak-coupling limit, the current is dominated by the contributions of first order in the coupling Γ . Because Γ already explicitly appears in Eq. (4.1), the Green's functions have to be calculated to zeroth order in Γ .³¹ The final result for the current can be written as a sum over two contributions,

$$I_r = I_r^P + I_r^S, \quad (4.2)$$

which explicitly contain either the occupation probabilities P_0, P_1, P_d or the accumulated spin \mathbf{S} , respectively,

$$I_r^P = \Gamma_r \frac{2(-e)}{\hbar} \left[f_r^+(\varepsilon) P_0 + \frac{f_r^+(\varepsilon + U) - f_r^-(\varepsilon)}{2} P_1 - f_r^-(\varepsilon + U) P_d \right], \quad (4.3)$$

$$I_r^S = -p_r \Gamma_r \frac{2(-e)}{\hbar} [f_r^-(\varepsilon) + f_r^+(\varepsilon + U)] \mathbf{S} \cdot \hat{\mathbf{n}}_r. \quad (4.4)$$

For nonmagnetic leads, only the term I_r^P contributes. At finite spin polarization in the leads, the additional term I_r^S appears, but also the first contribution I_r^P is affected via the modification of the occupation probabilities as given in Eq. (3.4).

In steady state the two currents I_L and I_R are connected by the conservation of charge on the dot, so the homogeneous current flowing through the system can be defined as $I = I_R = -I_L$.

V. RESULTS

In the following we discuss results for the spin accumulation and its impact on transport for both the linear and nonlinear regime. To be specific, we choose symmetric coupling $\Gamma_L = \Gamma_R = \Gamma/2$, equal spin polarizations $p_L = p_R = p$, and a symmetrically applied bias $V_R = -V_L = V/2$.

A. Linear response

In equilibrium, i.e., without any applied bias voltage, $V = 0$, no current flows and the stationary solution of the rate equations for the occupation probabilities (3.4) is given by the Boltzmann distribution, $P_\chi \sim \exp(-E_\chi/k_B T)$, and since in this case $(d\mathbf{S}/dt)_{\text{acc}} = 0$, no spin accumulation occurs in the quantum dot, $\mathbf{S} = 0$.³³

At nonzero bias voltage, a current flows through the system and spin is accumulated on the dot. To describe the dot state in the linear-response regime, $eV \ll k_B T$, we expand the steady-state solution of Eqs. (3.4) and (3.5) up to linear order in V . We find that (due to symmetric coupling) the dot occupation probabilities (P_0, P_1, P_d) have no corrections linear in V and are, thus, unchanged, independent of the size and direction of the leads magnetization. In contrast to the occupation probabilities, the source term for the spin accumulation has a nonzero contribution linear in V ,

$$\left(\frac{d\mathbf{S}}{dt}\right)_{\text{acc}} = \left[f'(\varepsilon) \left(P_0 + \frac{P_1}{2} \right) + f'(\varepsilon + U) \left(\frac{P_1}{2} + P_d \right) \right] \times \frac{p\Gamma}{\hbar} \frac{-eV}{2k_B T} (\hat{\mathbf{n}}_L - \hat{\mathbf{n}}_R), \quad (5.1)$$

generating a finite spin polarization along $\hat{\mathbf{n}}_L - \hat{\mathbf{n}}_R$, i.e., along the y axis. This is consistent with the notion of angular momentum conservation when magnetic moments polarized along $\hat{\mathbf{n}}_L$ enter from the left than those along $\hat{\mathbf{n}}_R$ leave the dot to the right.

The damping term, $(d\mathbf{S}/dt)_{\text{rel}} = -(\Gamma/\hbar) [f^-(\varepsilon) + f^+(\varepsilon + U)] \mathbf{S}$, limits the magnitude of spin accumulation, but it does not affect its direction. The third term, however, $(d\mathbf{S}/dt)_{\text{rot}} = \mathbf{S} \times (\mathbf{B}_L + \mathbf{B}_R)$ with $\mathbf{B}_r = \hat{\mathbf{n}}_r p\Gamma/(2\pi\hbar) \int' d\omega \left(\frac{1}{\omega - \varepsilon - U} - \frac{1}{\omega - \varepsilon} \right) f(\omega)$ and $\mathbf{B}_L + \mathbf{B}_R \equiv B_0 \cos(\phi/2) \hat{\mathbf{e}}_x$, yields a precession of the spin with an angle

$$\alpha = -\arctan \left(B_0 \tau_c \cos \frac{\phi}{2} \right) \quad (5.2)$$

about $\hat{\mathbf{n}}_L + \hat{\mathbf{n}}_R$, i.e., the x -axis. As a result, the accumulated spin acquires both y and z components as seen in Fig. 4. This precession acts back on the magnitude of the accumulated spin. The stationary solution of Eq. (3.10) yields $|\mathbf{S}| = \tau_c |(d\mathbf{S}/dt)_{\text{acc}}| \cos \alpha$, from which we infer that the precession is accompanied with a decrease of the spin accumulation.

The rotation angle α is plotted in Fig. 5(b) as a function of the level position ε . We see that α changes sign at $\varepsilon = -U/2$, which reflects a sign change of the exchange field at this point. The point $\varepsilon = -U/2$ is special, as in this case the system bears particle-hole symmetry. The fast variation of α in this region gives rise to a rather sharp feature in the magnitude of accumulated spin as a function of ε , see Fig. 5(c). The width of the emerging peak scales (for $k_B T < U/2$) with $\pi U [f^-(\varepsilon) + f^+(\varepsilon + U)]/[p \cos(\phi/2)]$, which can be even

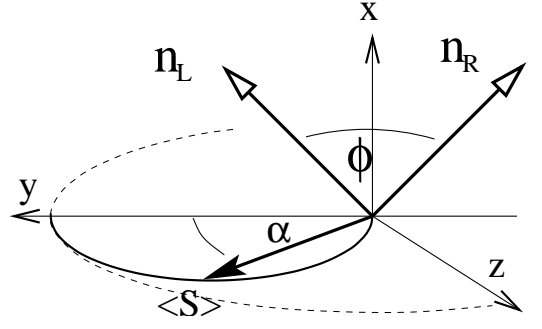


FIG. 4: Spin dynamics in the linear-response regime. Spin accumulates along the y direction. The spin precesses due to the exchange field that is along the x direction. Therefore, the stationary solution of the average spin on the dot is tilted away from the y axis by an angle α , plotted in Fig. 5(b).

smaller than temperature since the factor with the Fermi functions involved can become numerically small.

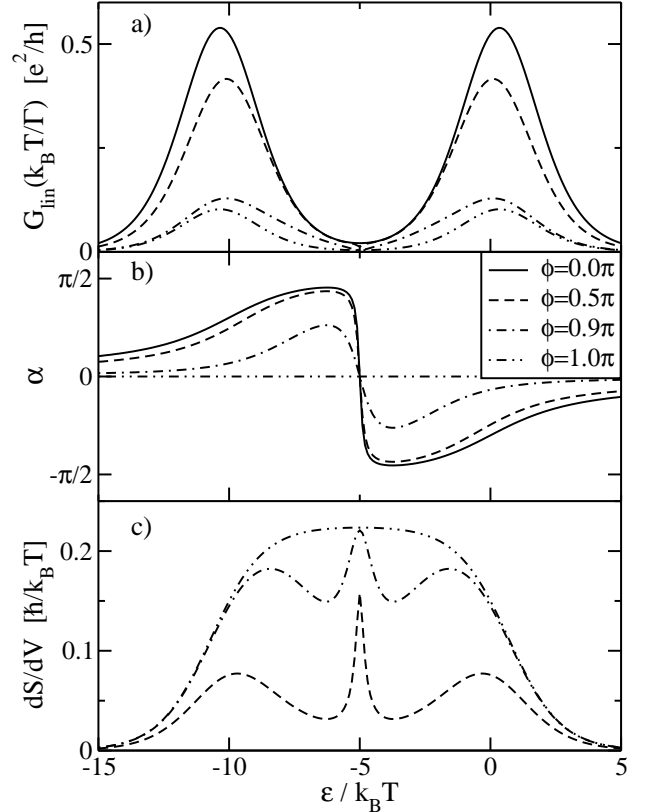


FIG. 5: (a) Linear conductance normalized by $\Gamma/k_B T$ as a function of the level position ε for different angles ϕ . (b) Angle α enclosed by the accumulated spin and the y axis as defined in Fig. 4. (c) Derivative of the magnitude of the accumulated spin on the dot with respect to the source-drain voltage V . Further parameters are $p = 0.9$ and $U = 10k_B T$.

As pointed out above, in the regime under considera-

tion the occupation probabilities do not depend on the spin polarization of the leads. In particular, they are independent of the relative angle ϕ of the leads' magnetization. This means that the ϕ dependence of the conductance will be completely determined by the product $\mathbf{S} \cdot \hat{\mathbf{n}}_L = -\mathbf{S} \cdot \hat{\mathbf{n}}_R$, as can be seen from Eqs. (4.3) and (4.4). It is the relative orientation of the accumulated spin and the drain (or source) that produces the ϕ dependence of the current, rather than the product $\hat{\mathbf{n}}_L \cdot \hat{\mathbf{n}}_R$, as in the case of a single magnetic tunnel junction. In this way, the ϕ dependent linear conductance $G^{\text{lin}} = (\partial I / \partial V)|_{V=0}$ directly reflects the accumulated spin. The effect of the exchange field \mathbf{B} is seen from the analytic expression

$$\frac{G^{\text{lin}}(\phi)}{G^{\text{lin}}(0)} = 1 - p^2 \frac{\sin^2(\phi/2)}{1 + (B_0 \tau_c)^2 \cos^2(\phi/2)}, \quad (5.3)$$

which is plotted in Fig. 6 for different values of the level position ε .

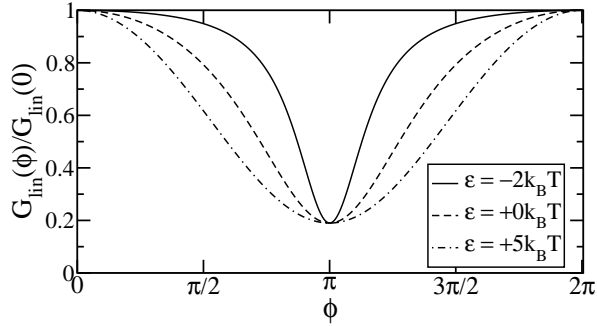


FIG. 6: Normalized conductance as a function of the angle ϕ enclosed by the lead magnetization for different level positions and the parameters $U = 10k_B T$ and $p = 0.9$.

For $\varepsilon > 0$, the quantum dot is predominantly empty, and for $\varepsilon + U < 0$ doubly occupied with a spin singlet. This is reflected by a small lifetime τ_c of a dot spin. Due to the short dwell time of a single spin-polarized electron in the dot, the rotation angle is small and the normalized conductance as a function of the relative angle ϕ of the lead magnetizations shows a harmonic behavior, see, e.g., the curve for $\varepsilon = 5k_B T$ in Fig. 6.

For $-U < \varepsilon < 0$, however, the dwell time is increased and the exchange field becomes important. It causes the above described spin precession, which decreases the product $\mathbf{S} \cdot \hat{\mathbf{n}}_L$ since the relative angle $\angle(\hat{\mathbf{n}}_L, \mathbf{S})$ is increased and the magnitude of \mathbf{S} is reduced. According to Eq. (4.4), the spin precession, thus, makes the spin-valve effect less pronounced, leading to a value of the conductance that exceeds the expectations made by Slonczewski⁶ for a single magnetic tunnel junction.

For parallel and antiparallel aligned lead magnetizations, $\phi = 0$ and $\phi = \pi$, the accumulated spin and the exchange field also get aligned. As a result, there is no spin precession, even though the exchange field is still present. For these cases, the ϕ -dependent conductance is not affected by the exchange field, see Fig. 6.

B. Nonlinear response

We now turn to the discussion of the non-linear response regime, $eV > k_B T$. In Fig. 7(a) we show the current I as a function of the bias voltage V for an antiparallel configuration of the leads' magnetizations and different values of the leads' spin polarization p . As it is

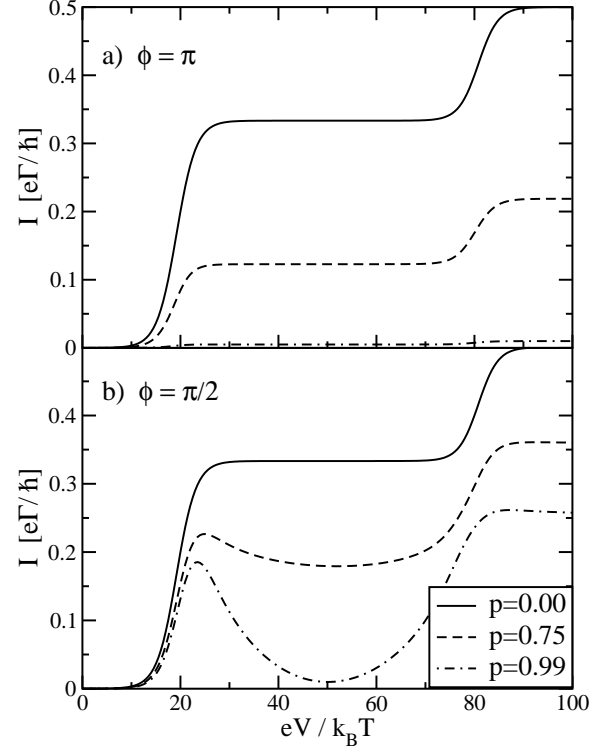


FIG. 7: Current-voltage characteristics for antiparallel (a) and perpendicular aligned (b) lead magnetizations. Further parameters are $\Gamma_L = \Gamma_R = \Gamma/2$, $p_L = p_R = p$, $\varepsilon = 10k_B T$, and $U = 30k_B T$.

well known from transport through quantum dots with nonmagnetic leads, the current increases in a steplike manner. At low bias voltage, the dot is always empty and transport is blocked. With increasing bias voltage, first single and then double occupancy of the dot is possible, which opens first one and then two transport channels. A finite spin polarization p leads to spin accumulation and, thus, to a reduction of transport. A reduction of transport with increasing p is also seen for noncollinear magnetization. There is a qualitative difference, though. As can be seen in Fig. 7(b), a very pronounced negative differential conductance evolves out of the middle plateau as the spin polarization p is increased.

Before explaining the origin of this negative differential conductance, we address the height of the plateau at large bias voltages first. Away from the steps, all appearing

Fermi functions are either 0 or 1. From Eq. (4.2) we get $I = (e\Gamma/2\hbar)[1 - p\mathbf{S} \cdot (\hat{\mathbf{n}}_L - \hat{\mathbf{n}}_R)]$. When the exchange field is ignored, which can be done here since the spin dwell time is shortened by the possibility of forming spin singlets, then the accumulated spin is $\mathbf{S} = p(\hat{\mathbf{n}}_L - \hat{\mathbf{n}}_R)/4$ from which we get

$$I = \frac{e\Gamma}{2\hbar} \left(1 - p^2 \sin^2 \frac{\phi}{2} \right). \quad (5.4)$$

The suppression of transport due to the spin polarization p of the leads is comparable with the case of a single-tunnel junctions, when charging effects are of no importance.

At intermediate bias voltages, the dot can be empty or singly occupied, but double occupation is forbidden. To understand the negative differential conductance we first neglect the exchange field and then, in a second step, analyze how the exchange field modifies the picture. Since double occupation of the dot is prohibited, all electrons entering the dot through the left barrier find an empty dot. This is consistent with the fact that the current $I = (e\Gamma/\hbar)P_0$ explicitly depends only on the probability to find the dot empty. The spin accumulation affects the current only indirectly via modifying P_0 . In the absence of the exchange field the relation between them is

$$\mathbf{S} = p \left[\frac{\Gamma_L}{\Gamma_R} P_0 \hat{\mathbf{n}}_L - \frac{1 - P_0}{2} \hat{\mathbf{n}}_R \right] \quad \text{with} \quad (5.5)$$

$$P_0 = \frac{1}{1 + 2\Gamma_L/\Gamma_R} \left[1 + \frac{4}{\Gamma_R/\Gamma_L + 2} \cdot \frac{p^2}{1 - p^2} \sin^2 \frac{\phi}{2} \right]^{-1} \quad (5.6)$$

(At this point we explicitly allow for different tunneling strengths.) As a consequence, with increasing ϕ and p the probability P_0 decreases, i.e., the dot is most of the time occupied with one electron, and the accumulated spin tends to align along $-\hat{\mathbf{n}}_R$, antiparallel to the drain electrode. The electron is, thus, trapped in the dot since tunneling out to the drain electrode is suppressed by a low density of states for the given spin direction. No second electron can enter the dot because of the Coulomb interaction, and transport is, thus, blocked. So this mechanism is a type of spin blockade but with a different physical origin compared to the systems described in literature.^{34,35}

The suppression factor coming from Eq. (5.6) defines the local minimum of the current in Fig. 7(b). At this point, the relevant exchange field component generated by the coupling to the left lead vanishes, so that spin precession becomes insignificant, see Fig. 9(a). Away from this point spin precession sets in as illustrated in Fig. 8. The spin rotates about $\hat{\mathbf{n}}_L$ and the electron can now more easily leave the dot via the drain electrode.

Similar to the linear-response regime, the rotation caused by the exchange field weakens the spin-valve effect. The two mechanisms, the spin blockade, and the spin precession have opposite effect on the spin-valve behavior. Together with the fact that the strength of the

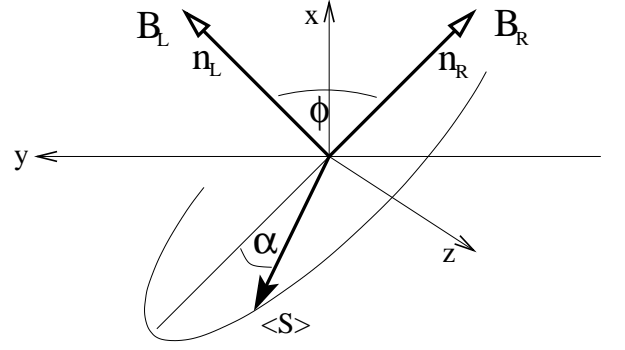


FIG. 8: For electrons polarized antiparallel to the drain lead, the influence of the effective field generated by the source lead is dominating. By rotating the spins, the spin blockade is lifted and therefore the conductance recovers.

exchange field varies as a function of the level position relative to the Fermi level, we now fully understand the origin of the nonlinear conductance. To illustrate this further, we plot in Fig. 9(b) the current which we obtain when we drop the contribution, Eq. (3.8), of the exchange field to the spin dynamics by hand and compare it with the full result. In the absence of the exchange field, a wide plateau is recovered, whose height is governed by Eq. (5.6). The peak at the left end of the plateau indicates that, once the dot level is close to the Fermi level of the source electrode, the spin blockade is relaxed since the dot electrons have the possibility to leave to the left side.

We now estimate under which circumstances the negative differential conductance will be visible. Since the spin-blockade mechanism is crucial for the negative differential conductance to form, the relevant criterion can be obtained from Eq. (5.6) as

$$\frac{4}{\Gamma_R/\Gamma_L + 2} \cdot \frac{p^2}{1 - p^2} \sin^2 \frac{\phi}{2} \sim 1, \quad (5.7)$$

i.e., for a typical value $\phi \approx \pi/2$ and symmetric coupling $\Gamma_L = \Gamma_R$ we need at least a spin polarization $p \approx 0.77$, in agreement with Fig. 7. An asymmetry in the coupling strength $\Gamma_L > \Gamma_R$ helps us to somewhat reduce the number of the required spin polarization.

The effect of the spin blockade on the ϕ -dependent current is depicted in Fig. 10. We choose the bias voltage according to $eV/2 = \varepsilon + U/2$, such that the influence of the exchange field is absent. For $p = 0.5$ still a $\sin^2 \frac{\phi}{2}$ dependence can be recognized. For higher polarizations the conductivity drops faster and stays nearly constant at its minimal value due to spin blockade. This is just the opposite behavior than predicted for the linear-response regime as seen in Fig. 6.

We close this section with the remark that while we plotted only results for the case $\varepsilon > 0$, in the opposite case $\varepsilon < 0$ the current-voltage characteristics is qualitatively the same.

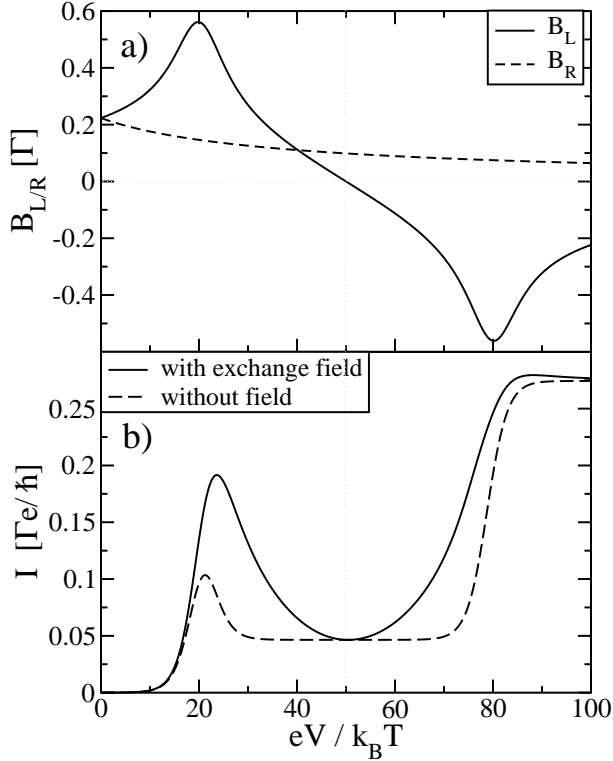


FIG. 9: Panel (a) The absolute value of the effective exchange field contributions from the left and right leads. Panel (b) the current voltage dependence, with and without the influence of the exchange field. For both plots the parameters $\phi = \pi/2$, $\Gamma_L = \Gamma_R = \Gamma/2$, $\varepsilon = 10k_B T$, $U = 30k_B T$, and $p = 0.95$ were chosen.

VI. EXTERNAL MAGNETIC FIELD

As we discussed in the previous section, the transport properties through the quantum dot crucially depend on the magnitude and direction of the average spin in the dot, which is determined by the interplay of spin-dependent tunneling and the effective exchange field. The application of an additional, external magnetic field \mathbf{B}_{ext} opens the possibility to manipulate the dot spin and, thus, the transport behavior in a direct way. Since the external magnetic field is independent of all the system parameters considered so far, the parameter space for experiments is enlarged by another dimension. Magnetic fields have been used either to split the energy levels for the different spin components¹⁸ or to rotate an accumulated spin.⁴² A combination of both, a static field splitting the energy levels plus an oscillating field to rotate the spin, defines an ESR scheme that allows for the study of single-spin dynamics in quantum dots in the absence of ferromagnetic leads, as proposed in Ref. 43.

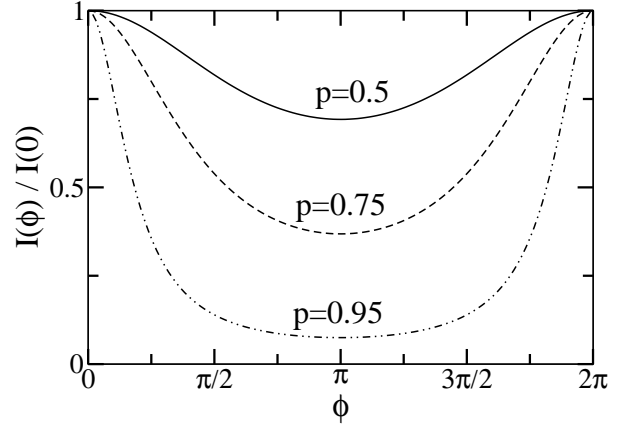


FIG. 10: Angular dependence of the conductance with an applied voltage of $V = \varepsilon + U/2$, i.e., the voltage generating the smallest influence of the exchange field. Further plot parameters are $\Gamma_L = \Gamma_R = \Gamma/2$, $p_L = p_R = p$, $\varepsilon = 10k_B T$, and $U = 30k_B T$.

The way a static external magnetic field affects the dot qualitatively depends on the ratio of the induced Zeeman energy and the intrinsic line width Γ of the dot energy levels.

A. Large Fields

At large magnetic fields, $B_{\text{ext}} \gg \Gamma$ (to keep the formulas transparent, we include the gyromagnetic factor in the definition of B_{ext}), all the complex spin dynamics discussed so far is absent. It is natural in this case to quantize the dot spin along the direction of \mathbf{B}_{ext} . The Zeeman splitting term $B_{\text{ext}} = \varepsilon_{\uparrow} - \varepsilon_{\downarrow}$ in the Liouville equation (3.2) ensures that for weak coupling, the density matrix always remains diagonal, as can be seen from expanding Eq. (3.2) to lowest order in Γ to obtain $0 = (\varepsilon_{\uparrow} - \varepsilon_{\downarrow})P_{\uparrow}^{\downarrow}$. As a consequence, the average spin on the dot is always polarized along the direction of the external magnetic field, and the exchange field does not play any role. In a physical picture, the spin components perpendicular to \mathbf{B}_{ext} are averaged out due to a fast precession movement. Transport effectively takes place through two energetically separated levels, where the coupling strength to the left and right leads depends on the angles $\theta_r = \angle(\mathbf{B}_{\text{ext}}, \hat{\mathbf{n}}_r)$ between the lead magnetizations and the external field via the relations $\Gamma_{r\uparrow} = \Gamma_r(1 + p_r \cos \theta_r)$ and $\Gamma_{r\downarrow} = \Gamma_r(1 - p_r \cos \theta_r)$. Thereby we assumed that the applied magnetic field is not strong enough to tilt the lead magnetization direction. It is worth to point out that the spin polarization and the trigonometric function of the relative angle θ_r appear always as a product, so that this system is equivalent

to the collinear cases^{12,18} with decreased magnetization of the leads.

B. Small Fields

The situation becomes more interesting in the limit of small fields, $B_{\text{ext}} \lesssim \Gamma$. To describe this case, we perform the same perturbation expansion in Γ as before, but count B_{ext} as being first order in Γ . This introduces in Eq. (3.2) the (first-order) term $(\varepsilon_{\uparrow} - \varepsilon_{\downarrow})P_{\uparrow}^{\downarrow}$, while the kernels Σ are then not affected by the external magnetic field, because they are already of first order in the coupling strength Γ .

It turns out that, in the considered limit, the only change introduced by the external magnetic field is an additional term $\mathbf{S} \times \mathbf{B}_{\text{ext}}$ in the Bloch-like equation

$$\frac{d\mathbf{S}}{dt} = \left(\frac{d\mathbf{S}}{dt}\right)_{\text{acc}} + \left(\frac{d\mathbf{S}}{dt}\right)_{\text{rel}} + \mathbf{S} \times \mathbf{B} \quad (6.1)$$

with $\mathbf{B} = \mathbf{B}_L + \mathbf{B}_R + \mathbf{B}_{\text{ext}}$. With the external magnetic field as a new parameter all the effects of spin blockade and the precession discussed so far can be enhanced or suppressed and made independent of the lead alignment.

An external field is applied along $\hat{\mathbf{e}}_x = (\hat{\mathbf{n}}_L + \hat{\mathbf{n}}_R)/|\hat{\mathbf{n}}_L + \hat{\mathbf{n}}_R|$ leads to a suppression of the spin-valve effect in the linear-response regime similarly as due to exchange field. In fact, according to Eq. (6.1) the magnitude of the relevant field is just the sum of the exchange and the external fields. The linear conductance as a function of B_{ext} is displayed in Fig. 11. In the absence of the effec-

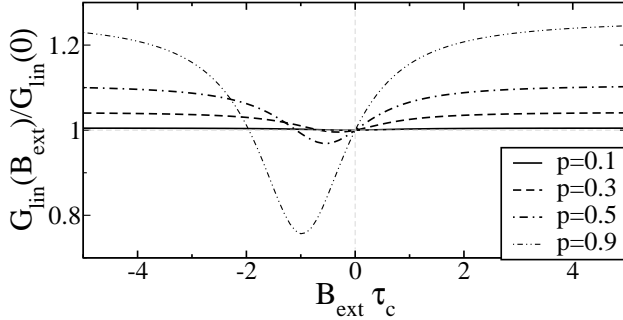


FIG. 11: Linear conductance as a function of an applied external magnetic field in x direction. The parameters are $\Gamma_L = \Gamma_R = \Gamma/2$, $p_L = p_R = p$, $\varepsilon = 0$, $U = 10k_B T$, and $\phi = \pi/2$.

tive exchange field the conductance would be symmetric around $B_{\text{ext}} = 0$, and any value of the field would increase the conductance as discussed in Sec. V A. The exchange field yields a shift of the position of the minimum. This opens the possibility to determine the exchange field experimentally by changing the external magnetic field and keeping all other parameters fixed. From the generalization of Eq. (5.3) to the present case it becomes apparent

that the width of the minimum is given by the inverse of the dwell time τ_c in the dot, since during this time the dot spin is influenced by the fields.

We remark that the effect of external-field components perpendicular to the x direction is somewhat more complicated, even in the linear-response regime. The reason is that the induced precession will generate some finite spin accumulation along the x direction, which introduces a linear correction in V of the charge occupation probabilities via Eq. (3.4). This, in turn, acts back on the accumulated spin due to Eq. (3.6).

VII. INCLUSION OF SPIN RELAXATION

We emphasize that the only source of spin relaxation considered in our analysis is the tunnel coupling of the dot states to the left and right leads, i.e., we require that the spin-flip relaxation time due to other mechanisms such as coupling to nuclear spins,³⁷ or spin-orbit coupling³⁸ is large enough not to destroy spin accumulation. If we assume a spin relaxation rate T_2 equal to the ensemble spin dephasing time $T_2^* \approx 100 \text{ ns}$ for n-doped GaAs bulk material³⁹ as lower boundary, it is still justifiable to neglect spin relaxation effects for interface resistances of the order of $1M\Omega$.⁴⁰ But recent measurements with semiconducting quantum dots indicate even much longer spin relaxation times.⁴¹

Nevertheless, (extrinsic) spin relaxation can be the most limiting factor for various spin-accumulation experiments in systems of larger size.^{36,42} To include extrinsic spin relaxation in a simplified phenomenological way, we add an isotropic relaxation term $-\mathbf{S}/\tau_{\text{ext}}$ in Eq. (3.7), which leads to

$$\left(\frac{d\mathbf{S}}{dt}\right)_{\text{rel}} = -\frac{1}{\tau_s}\mathbf{S} = -\left(\frac{1}{\tau_c} + \frac{1}{\tau_{\text{ext}}}\right)\mathbf{S}. \quad (7.1)$$

Now, two characteristic time scales have to be distinguished: the average time an electron stays in the dot, τ_c , and the meanlife time of a dot spin, $\tau_s = (1/\tau_c + 1/\tau_{\text{ext}})^{-1}$.

By solving the system of master equations for the linear-response regime, we see that we have to replace the factor τ_c with τ_s everywhere in the previous discussions, which matches the intuition that τ_s is the relevant time scale for spin related effects. From Eq. (3.10) we see that the extrinsic relaxation processes reduce the magnitude of the spin accumulation by a factor τ_s/τ_c . The observation that the accumulated spin on the dot and, therefore, all spin related effects in transport vanish linearly with τ_s/τ_c (and not exponentially) implies that magnetoresistance effects can still be measured, even if the mean dwell time of the electrons in the dot exceeds the spinlife time significantly, which was experimentally confirmed by Ref. 42. The reason for the linear dependence is the following. Even when the spins relax much faster than the mean dwell time, a fraction of the spins

leaves the dot already before being relaxed. The probability of detecting a spin with the original alignment in a transport measurement is given by the time integral $P_{\text{spin}} = \int_0^\infty dt \exp(-t/\tau_s)/\tau_c = \tau_s/\tau_c$, which is linear despite the exponential decay of the accumulated spin on the dot.

VIII. RELATION TO SPIN-MIXING CONDUCTANCE

Transport through multiterminal devices with noncollinear lead magnetizations has been discussed recently by using the language of a complex spin-mixing conductance $G_{\uparrow\downarrow}$ within a circuit theory.²³ The mixing conductance $G_{\uparrow\downarrow}$ contains the information about the transport of spins oriented perpendicular to the magnetization of the ferromagnetic leads. Using this approach, the conductance of a two-terminal device with noncollinear magnetization of the leads can be described in linear response by the general relation

$$G(\theta) = \frac{G}{2} \left(1 - p^2 \frac{\tan^2(\theta/2)}{\tan^2(\theta/2) + |\eta|^2/\text{Re}\eta} \right), \quad (8.1)$$

where $\eta \equiv 2G_{\uparrow\downarrow}/G$ is the complex spin-mixing conductance normalized to the sum G of the spin-up and spin-down conductance of a single contact. This formula, Eq. (8.1), is quite general but requires the knowledge of η . Hybrid systems of ferromagnets with normal metals in diffusive and ballistic regime²³ or even Luttinger liquids^{44,45} have been described. For system with tunnel contacts $\text{Re}\eta = 1$ and Eq. (5.3) can be transformed into the form Eq. (8.1) by identifying

$$\text{Im}\eta \equiv \frac{2\text{Im}G_{\uparrow\downarrow}}{G} = B_0\tau_c. \quad (8.2)$$

Our approach, thus, provides a theory for the interaction effects on the spin-mixing conductance in the linear-response regime. The imaginary part $\text{Im}\eta$ is proportional to the local effective field experienced by the dot spins, because this field is responsible for the spin precession which yields a coherent mixing of the two spin channels.

IX. CONCLUSIONS

In the presented work the influence of charging interaction effects on the tunnel magnetoresistance for systems with noncollinearly magnetized leads has been discussed. We examined a single-level quantum connected to ferromagnetic leads as a model system and found that charge- and spin-related properties do not just coexist but their interplay gives rise to new effects detectable in transport measurements.

The most important effects discussed in this paper are related to the existence of an effective exchange magnetic field $\mathbf{B}_L + \mathbf{B}_R$, which leads to a precession movement of

the accumulated spin on the dot. This precession weakens the spin-valve effect by reducing the amount of accumulated spin and changing its orientation relative to the leads. As a result, the current flowing through the system is increased due to the exchange field. Also the functional form of the angular-dependent linear conductance is affected, and the cos-dependence valid for a single magnetic tunnel junction is modified due to the precession of the accumulated spin.

In nonlinear response, the accumulated spin on the dot tends to align antiparallel to the drain lead magnetization. Such a spin blockade causes a suppression of transport for the bias-voltage regime in which the dot can be empty or singly occupied. The spin precession due to the coupling to ferromagnetic leads countersteers the spin blockade by tilting the spin accumulation direction. Since the strength of the exchange field is a nonmonotonic function of the applied voltage, a regime with negative differential conductance exists.

Attaching ferromagnetic leads to quantum dots is quite challenging. One promising approach is to contact an ultrasmall aluminum nanoparticle, which serves as a quantum dot, to ferromagnetic metallic electrodes. In this way, quantum dots with one magnetic and one nonmagnetic electrode have already been fabricated.¹⁸ An alternative idea is to use carbon nanotubes as quantum dots and to place them on ferromagnetic contacts.¹⁰ But also other systems are conceivable, such as self-assembled InAs quantum dots in GaAs LEDs with (Ga,Mn)As as ferromagnetic electrode,¹⁷ or STM setups with a natural or artificial impurity on a ferromagnetic substrate contacted by a ferromagnetic STM tip.⁴⁶

Acknowledgments

We thank J. Barnaś, G. Bauer, A. Brataas, S. Maekawa, G. Schön, and D. Urban for discussions. This work was supported by the Deutsche Forschungsgemeinschaft under the Emmy-Noether program and the Center for Functional Nanostructures, through SFB491 and GRK726, by the EC under the Spintronics Network RTN2-2001-00440, and the Center of Excellence for Magnetic and Molecular Materials for Future Electronics G5MA-CT-2002-04049 and Project PBZ/KBN/044/P03/2001.

APPENDIX A: DIAGRAMMATIC TECHNIQUE

In this appendix we present some technical details of the derivation of the master equations and the transport current. The approach is based on the diagrammatic technique developed in Ref. 25, designed for the application in quantum dot systems. The actual calculation is to some degree similar to transport through Aharonov-Bohm interferometers with quantum dots.²⁴

1. Transition rates Σ

In the Liouville equation (3.2) the transition rates appear as irreducible self-energies $\Sigma_{\chi_2' \chi_2}^{\chi_1' \chi_1}$. These self-energy parts are represented as block diagrams enclosed by a Keldysh contour. Examples of first-order diagrams are shown in Fig. 12. The real-time axis runs horizontally from the left to the right while the upper (lower) line represents the forward (backward) propagator of the dot on a Keldysh time contour. The rules to calculate the Σ

$$\begin{aligned} \Sigma_{0\downarrow}^{0\uparrow} &= \begin{array}{c} \text{Diagram 1: } 0 \xrightarrow{\uparrow} \uparrow, 0 \xrightarrow{\downarrow} \downarrow, \text{dashed line } \uparrow \rightarrow \downarrow \text{ with } (\uparrow) \text{ and } (\downarrow) \\ \text{Diagram 2: } 0 \xrightarrow{\uparrow} \uparrow, 0 \xrightarrow{\downarrow} \downarrow, \text{dashed line } \downarrow \rightarrow \uparrow \text{ with } (\downarrow) \text{ and } (\uparrow) \end{array} + \\ \Sigma_{dd}^{dd} &= \sum_{\sigma} \left\{ \begin{array}{c} \text{Diagram 3: } d \xrightarrow{\sigma} d, d \xrightarrow{\bar{\sigma}} d, \text{dashed line } d \rightarrow d \text{ with } \sigma \text{ and } \bar{\sigma} \\ \text{Diagram 4: } d \xrightarrow{\bar{\sigma}} d, d \xrightarrow{\sigma} d, \text{dashed line } d \rightarrow d \text{ with } \bar{\sigma} \text{ and } \sigma \end{array} \right\} \\ \Sigma_{\uparrow\downarrow}^{\uparrow\downarrow} &= \begin{array}{c} \text{Diagram 5: } \uparrow \xrightarrow{0} \downarrow, \uparrow \xrightarrow{d} \downarrow, \text{dashed line } \uparrow \rightarrow \downarrow \text{ with } (\uparrow) \text{ and } (\downarrow) \\ \text{Diagram 6: } \uparrow \xrightarrow{d} \downarrow, \uparrow \xrightarrow{0} \downarrow, \text{dashed line } \downarrow \rightarrow \uparrow \text{ with } (\downarrow) \text{ and } (\uparrow) \end{array} + \end{aligned}$$

FIG. 12: Examples for the diagrams representing the generalized transition rates Σ .

are:²⁵

1.) Draw all topologically different diagrams with tunneling lines connecting vertices on either the same or opposite propagators. Assign to the four corners and all propagators the states $\chi = 0, \uparrow, \downarrow, d$ and the corresponding energies ε_{χ} , as well as an energy ω to each tunneling line.

2.) For each time interval on the real axis confined by two neighboring vertices, assign the resolvent $1/(\Delta E + i0^+)$, where ΔE is the energy difference between left and right going tunnel lines and propagators.

3.) For each vertex connecting a double-occupied state d to the up state \uparrow , the diagram acquires a factor (-1) .

4.) Assign to each tunneling line the factor $\gamma_{\sigma\sigma'}^+(\omega)$ [$\gamma_{\sigma\sigma'}^-(\omega)$] when the tunneling line is going backward (forward) with respect to the Keldysh contour. Its form is

$$\gamma_{\sigma\sigma'}^{\pm}(\omega) = \frac{1}{2\pi} \sum_{r, \chi=\pm} \frac{\Gamma_{r\chi}}{2} f_r^{\pm}(\omega), \quad (\text{A1})$$

$$\begin{aligned} \gamma_{\uparrow\downarrow}^{\pm}(\omega) &= \frac{1}{4\pi} (\Gamma_{L+} f_L^{\pm} e^{i\phi/2} + \Gamma_{R+} f_R^{\pm} e^{-i\phi/2} \\ &\quad - \Gamma_{L-} f_L^{\pm} e^{i\phi/2} - \Gamma_{R-} f_R^{\pm} e^{-i\phi/2}) \quad (\text{A2}) \\ &= \gamma_{\uparrow\downarrow}^{\pm*}(\omega). \end{aligned}$$

Here, σ and σ' are the spins of the electron that leaves and enters the vertices connected by the line. The factors $\gamma^{\pm}(\omega)$ come from the contraction of two lead operators in the tunnel Hamiltonian and resemble the transition rates predicted by Fermi's golden rule, including a sum

over all intermediate lead states ($r = R/L, \sigma = +/ -$). Dependent on the time ordering, the transition rate is proportional to the electron f^+ or the hole distribution function $f^- = 1 - f^+$, while the relative phases can be extracted from Fig. 3.

5.) The diagram gets a prefactor of $(-1)^b(-1)^c$, where b is number of internal vertices on the backward propagator, and c the number of crossings of tunnel lines.

6.) Integrate over all energies of the tunneling lines.

In the sequential-tunneling regime, only one tunnel line per diagram is involved. Therefore, only one frequency integral appears which can be calculated trivially by using Cauchy's formula.

2. Green's functions

For the calculation of the transport current, we need the Fourier transform of the Keldysh Green's functions,

$$G_{\sigma\sigma'}^>(t) = -i \langle c_{\sigma}(t) c_{\sigma'}^{\dagger}(0) \rangle, \quad (\text{A3})$$

$$G_{\sigma\sigma'}^<(t) = +i \langle c_{\sigma'}^{\dagger}(0) c_{\sigma}(t) \rangle. \quad (\text{A4})$$

The Green's function is an average of one creation and

$$\begin{aligned} G_{\uparrow\downarrow}^> &= P_{\uparrow\downarrow}^{\cdot} \left(\begin{array}{c} \text{Diagram 1: } \uparrow \xrightarrow{d} \downarrow, \text{dashed line } \uparrow \rightarrow \downarrow \text{ with } (\uparrow) \text{ and } (\downarrow) \\ \text{Diagram 2: } \uparrow \xrightarrow{d} \downarrow, \text{dashed line } \downarrow \rightarrow \uparrow \text{ with } (\downarrow) \text{ and } (\uparrow) \end{array} \right) \\ G_{\uparrow\downarrow}^< &= - \left\{ P_{\uparrow\downarrow}^{\cdot} \left(\begin{array}{c} \text{Diagram 3: } \uparrow \xrightarrow{0} \downarrow, \text{dashed line } \uparrow \rightarrow \downarrow \text{ with } (\uparrow) \text{ and } (\downarrow) \\ \text{Diagram 4: } \uparrow \xrightarrow{0} \downarrow, \text{dashed line } \downarrow \rightarrow \uparrow \text{ with } (\downarrow) \text{ and } (\uparrow) \end{array} \right) + P_{\uparrow\downarrow}^{\cdot} \left(\begin{array}{c} \text{Diagram 5: } \uparrow \xrightarrow{d} \downarrow, \text{dashed line } \uparrow \rightarrow \downarrow \text{ with } (\downarrow) \text{ and } (\uparrow) \\ \text{Diagram 6: } \uparrow \xrightarrow{d} \downarrow, \text{dashed line } \downarrow \rightarrow \uparrow \text{ with } (\uparrow) \text{ and } (\downarrow) \end{array} \right) \right\} \\ G_{\sigma\sigma}^> &= P_{\bar{\sigma}}^{\cdot} \left(\begin{array}{c} \text{Diagram 7: } \bar{\sigma} \xrightarrow{d} \bar{\sigma}, \text{dashed line } \bar{\sigma} \rightarrow \bar{\sigma} \text{ with } (\sigma) \text{ and } (\bar{\sigma}) \\ \text{Diagram 8: } \bar{\sigma} \xrightarrow{d} \bar{\sigma}, \text{dashed line } \bar{\sigma} \rightarrow \bar{\sigma} \text{ with } (\bar{\sigma}) \text{ and } (\sigma) \end{array} \right) + P_{\bar{\sigma}}^{\cdot} \left(\begin{array}{c} \text{Diagram 9: } \bar{\sigma} \xrightarrow{0} \bar{\sigma}, \text{dashed line } \bar{\sigma} \rightarrow \bar{\sigma} \text{ with } (\sigma) \text{ and } (\bar{\sigma}) \\ \text{Diagram 10: } \bar{\sigma} \xrightarrow{0} \bar{\sigma}, \text{dashed line } \bar{\sigma} \rightarrow \bar{\sigma} \text{ with } (\bar{\sigma}) \text{ and } (\sigma) \end{array} \right) + P_0^{\cdot} \left(\begin{array}{c} \text{Diagram 11: } 0 \xrightarrow{\sigma} 0, \text{dashed line } 0 \rightarrow 0 \text{ with } (\sigma) \text{ and } (\sigma) \\ \text{Diagram 12: } 0 \xrightarrow{\sigma} 0, \text{dashed line } 0 \rightarrow 0 \text{ with } (\sigma) \text{ and } (\sigma) \end{array} \right) + P_0^{\cdot} \left(\begin{array}{c} \text{Diagram 13: } 0 \xrightarrow{\sigma} 0, \text{dashed line } 0 \rightarrow 0 \text{ with } (\sigma) \text{ and } (\sigma) \\ \text{Diagram 14: } 0 \xrightarrow{\sigma} 0, \text{dashed line } 0 \rightarrow 0 \text{ with } (\sigma) \text{ and } (\sigma) \end{array} \right) \end{aligned}$$

FIG. 13: Examples for the diagrams representing Green's functions.

one annihilation operator. These operators appear as external vertices (open circles) in the diagrams. They can be constructed following the rules:

1.) Draw the bare contour, the external vertices, and the virtual tunnel line in the proper orientation as seen in Fig. 13. The indices of the Green's function indicate the spin of the created and annihilated electrons at the external vertices. If higher-order contributions in Γ are to be calculated, add internal vertices according to the desired order and connect them by tunnel lines. Multiply the diagram with the matrix element of the density matrix corresponding to the initial state. Assign to each propagator with state χ the corresponding energy ε_{χ} and to each tunnel line and the virtual line an energy ω .

- 2.) Apply the same rule as no.(2) for calculating Σ .
- 3.) Apply the same rule as no.(3) for calculating Σ .
- 4.) Assign each tunneling line the factor $(-1)^v \gamma_{\sigma\sigma'}^+(\omega)$, where v is the number of external vertices on the Keldysh contour enclosed by the end points of the tunnel line. The line connecting the external vertices does not contribute.
- 5.) Apply the same rule as no.(5) for calculating Σ .
- 6.) Integrate over all energies except the energy assigned to the virtual tunnel line.

For the lesser function $G_{\sigma\sigma'}^<$, the direction of the external tunnel lines is reversed, and an additional global minus sign is involved in the definition.

In this paper we assume weak dot-lead coupling, i.e., we need only the zeroth-order Green's functions. In this limit, we get $G_{\sigma\sigma}^>(\omega) = -2\pi i P_{\sigma} \delta(\omega - \varepsilon - U) - 2\pi i P_0 \delta(\omega - \varepsilon)$, $G_{\sigma\sigma}^<(\omega) = +2\pi i P_{\sigma} \delta(\omega - \varepsilon) + 2\pi i P_d \delta(\omega - \varepsilon - U)$ and for $\sigma \neq \bar{\sigma}$ we find $G_{\sigma\bar{\sigma}}^>(\omega) = 2\pi i P_{\sigma}^{\sigma} \delta(\omega - \varepsilon - U)$, $G_{\sigma\bar{\sigma}}^<(\omega) = 2\pi i P_{\sigma}^{\sigma} \delta(\omega - \varepsilon)$.

-
- ¹ G. Prince, Science **282**, 1660 (1998).
 - ² S. Datta and B. Das, Appl. Phys. Lett. **56**, 665 (1990).
 - ³ M. N. Baibich, J. M. Broto, A. Fert, F. Nguyen Van Dau, F. Petroff, P. Etienne, G. Creuzet, A. Friederich, and J. Chazelas, Phys. Rev. Lett. **61**, 2472 (1988).
 - ⁴ M. Jullière, Phys. Lett. A **54**, 225 (1975).
 - ⁵ J. S. Moodera and L. R. Kinder, J. Appl. Phys. **79**, 4724 (1996); H. Jaffrès, D. Lacour, F. Nguyen Van Dau, J. Briatico, F. Petroff, and A. Vaurès, Phys. Rev. B **64**, 064427 (2001).
 - ⁶ J. C. Slonczewski, Phys. Rev. B **39**, 6995 (1989).
 - ⁷ J. Barnaś and A. Fert, Phys. Rev. Lett. **80**, 1058 (1998); S. Takahashi and S. Maekawa, Phys. Rev. Lett. **80**, 1758 (1998); A. Brataas, Yu. V. Nazarov, J. Inoue, and G. E. W. Bauer, Phys. Rev. B **59**, 93 (1999); J. Barnaś, J. Martinek, G. Michałek, B. R. Bułka, and A. Fert, Phys. Rev. B **62**, 12363 (2000); J. Martinek, J. Barnaś, S. Maekawa, H. Schoeller, and G. Schön, Phys. Rev. B **66**, 014402 (2002).
 - ⁸ K. Ono, H. Shimada, and Y. Ootuka, J. Phys. Soc. Jpn. **66**, 1261 (1997).
 - ⁹ L. F. Schelp, A. Fert, F. Fettar, P. Holody, S. F. Lee, J. L. Maurice, F. Petroff, and A. Vaurès, Phys. Rev. B **56**, R5747 (1997); K. Yakushiji, S. Mitani, K. Takanashi, S. Takahashi, S. Maekawa, H. Imamura, and H. Fujimori, Appl. Phys. Lett. **78**, 515 (2001).
 - ¹⁰ A. Jensen, J. Nygård and J. Borggreen in *Proceedings of the International Symposium on Mesoscopic Superconductivity and Spintronics*, edited by H. Takayanagi and J. Nitta, (World Scientific 2003), pp. 33-37; B. Zhao, I. Mönch, H. Vinzelberg, T. Mühl, and C. M. Schneider, Appl. Phys. Lett. **80**, 3144 (2002); K. Tsukagoshi, B. W. Alphenaar, and H. Ago, Nature **401**, 572 (1999).
 - ¹¹ J. König and J. Martinek, Phys. Rev. Lett. **90**, 166602 (2003).
 - ¹² W. Rudziński and J. Barnaś, Phys. Rev. B **64**, 085318 (2001).
 - ¹³ A. Cottet, W. Belzig, and C. Bruder, Phys. Rev. Lett. **92**, 206801 (2004); A. Cottet and W. Belzig, Europhys. Lett. **66**, 405 (2004); A. Cottet, W. Belzig, and C. Bruder, Phys. Rev. B **70**, 115315 (2004).
 - ¹⁴ G. Usaj and H. U. Baranger, Phys. Rev. B **63**, 184418 (2001).
 - ¹⁵ J. Martinek, Y. Utsumi, H. Imamura, J. Barnaś, S. Maekawa, J. König, and G. Schön, Phys. Rev. Lett. **91**, 127203 (2003); J. Martinek, M. Sindel, L. Borda, J. Barnaś, J. König, G. Schön, and J. von Delft, Phys. Rev. Lett. **91**, 247202 (2003).
 - ¹⁶ J. Fransson, O. Eriksson, and I. Sandalov, Phys. Rev. Lett. **88**, 226601 (2002);
 - ¹⁷ Y. Chye, M. E. White, E. Johnston-Halperin, B. D. Gerardot, D. D. Awschalom, and P. M. Petroff, Phys. Rev. B **66**, 201301(R) (2002).
 - ¹⁸ M. M. Deshmukh and D. C. Ralph, Phys. Rev. Lett. **89**, 266803 (2002).
 - ¹⁹ M.-S. Choi, D. Sánchez, and R. López, Phys. Rev. Lett. **92**, 056601 (2004); B. G. Wang, J. Wang, and Hong Guo, J. Phys. Soc. Jpn. **70**, 2645 (2001); N. Sergueev, Q. F. Sun, H. Guo, B. G. Wang, and J. Wang, Phys. Rev. B **65**, 165303 (2002).
 - ²⁰ D. Mozyrsky, L. Fedichkin, S. A. Gurvitz, and G. P. Berman, Phys. Rev. B **66**, 161313 (2002); J.-X. Zhu and A. V. Balatsky, Phys. Rev. Lett. **89**, 286802 (2002); Phys. Rev. B **67**, 174505 (2003); L. N. Bulaevskii, M. Hruška, and G. Ortiz, Phys. Rev. B **68**, 125415 (2002); L. N. Bulaevskii and G. Ortiz, Phys. Rev. Lett. **90**, 040401 (2003); A. V. Balatsky, Y. Manassen, and R. Salem, Phys. Rev. B **66**, 195416 (2002).
 - ²¹ Y. Manassen, R. J. Hamers, J. E. Demuth, and A. J. Castellano, Phys. Rev. Lett. **62**, 2531 (1989); C. Durkan and M. E. Welland, Appl. Phys. Lett. **80**, 458 (2002).
 - ²² In the opposite limit, i.e., strong dot-lead coupling, Kondo correlations may arise. Their interplay with ferromagnetism in the leads has been discussed in Refs. 15.
 - ²³ A. Brataas, Y. V. Nazarov, and G. E. W. Bauer, Eur. Phys. J B **22**, 99 (2001); D. H. Hernando, Y. V. Nazarov, A. Brataas and G. E. W. Bauer, Phys. Rev. B **62**, 5700 (2000).
 - ²⁴ J. König and Y. Gefen, Phys. Rev. Lett. **86**, 3855 (2001); Phys. Rev. B **65**, 045316 (2002).
 - ²⁵ J. König, H. Schoeller, and G. Schön, Phys. Rev. Lett. **76**, 1715 (1996); J. König, J. Schmid, H. Schoeller, and G. Schön, Phys. Rev. B **54**, 16820 (1996); H. Schoeller, in *Mesoscopic Electron Transport*, edited by L. L. Sohn, L. P. Kouwenhoven, and G. Schön (Kluwer, Dordrecht, 1997); J. König, *Quantum Fluctuations in the Single-Electron Transistor* (Shaker, Aachen, 1999).
 - ²⁶ D. V. Averin, A. N. Korotkov, and K. K. Likharev, Phys. Rev. B **44**, 6199 (1991); C. W. J. Beenakker, Phys. Rev. B **44**, 1646 (1991).
 - ²⁷ *The Kondo Problem to Heavy fermions*, edited by A.C. Hewson (Cambridge Press, 1993).
 - ²⁸ J. König, J. Martinek, J. Barnaś, and G. Schön, cond-mat/0404509.
 - ²⁹ J. Martinek, M. Sindel, L. Borda, J. Barnaś, R. Bulla, J. König, G. Schön, S. Maekawa, and J. von Delft, cond-mat/0406323.
 - ³⁰ Y. Meir and N. S. Wingreen, Phys. Rev. Lett. **68**, 2512 (1992).
 - ³¹ We would like to point out that, for nonvanishing bias voltage, the zeroth-order Green's function is *not* the equilib-

rium Green's function of the isolated dot. As calculated in Appendix A 2, the zeroth-order Green's function depends on the dot's charge and spin occupation which is determined by solving the system of master equations, Eqs. (3.4) and (3.5). While the master equations, Eqs. (3.4) and (3.5), contain the transition rates in first order in Γ , the solutions for P_0 , P_1 , P_d , and \mathbf{S} are of zeroth order and so is the Green's function. Nevertheless the latter depend on the leads' properties via the first-order rates in the master equation.

- ³² There is no splitting when the exchange field vanishes. In linear response and for $p_L = p_R$, $\Gamma_L = \Gamma_R$, this is the case either for antiparallel magnetized leads, $\hat{\mathbf{n}}_L = -\hat{\mathbf{n}}_R$, or when the integral in Eq. (3.9) has a zero. At this zero, the two terms associated with electron like and hole like processes cancel each other. With our assumption of a constant density of states, this situation is reached for $2\varepsilon + U = 0$, then the system bears a particle-hole symmetry.
- ³³ We emphasize that this absence of spin accumulation is a peculiarity of the weak-coupling limit. Corrections of higher order in the coupling strength Γ will yield a net spin accumulation due to the spin-dependent energy level renormalization discussed in the previous section, but this is beyond the scope of this paper.
- ³⁴ D. Weinmann, W. Häusler, and B. Kramer, Phys. Rev. Lett. **74**, 984 (1995); A. K. Huettel, H. Qin, A. W. Holleitner, R. H. Blick, K. Neumaier, D. Weinmann, K. Eberl, and J. P. Kotthaus, Europhys. Lett. **62**, 712 (2003).

- ³⁵ K. Ono, D. G. Austing, Y. Tokura, and S. Tarucha, Science **297**, 1313 (2002).
- ³⁶ M. Johnson and R. H. Silsbee, Phys. Rev. Lett. **55**, 1790 (1985); Phys. Rev. B. **37**, 5326 (1988).
- ³⁷ S. I. Erlingsson and Y. V. Nazarov Phys. Rev. B **66**, 155327 (2002); I. A. Merkulov, A. L. Efros, and M. Rosen, Phys. Rev. B, **65**, 205309; A. V. Khaetskii, D. Loss, and L. Glazman, Phys. Rev. Lett. **88**, 186802 (2002).
- ³⁸ A. V. Khaetskii and Y. V. Nazarov, Phys. Rev. B **64**, 125316 (2001); V. N. Golovach, A. Khaetskii, and D. Loss, Phys. Rev. Lett. **93**, 016601 (2004);
- ³⁹ J. M. Kikkawa and D. D. Awschalom, Phys. Rev. Lett. **80**, 4313 (1998).
- ⁴⁰ M. M. Deshmukh, E. Bonet, A. N. Pasupathy, and D. C. Ralph, Phys. Rev. B, **65**, 073301 (2002).
- ⁴¹ T. Fujisawa, D. G. Austing, Y. Tokura, Y. Hirayama, and S. Tarucha, Phys. Rev. Lett. **88**, 236802 (2002).
- ⁴² M. Zaffalon and B. J. van Wees, Phys. Rev. Lett. **91**, 186601 (2003).
- ⁴³ P. Recher, E. V. Sukhorukov, and D. Loss, Phys. Rev. Lett. **85**, 1962 (2000); H. A. Engel and D. Loss, Phys. Rev. Lett. **86**, 4648 (2001); Phys. Rev. B **65**, 195321-1 (2002).
- ⁴⁴ L. Balents and R. Egger, Phys. Rev. Lett. **85**, 3464 (2000); Phys. Rev. B **64**, 035310 (2001).
- ⁴⁵ M. Y. Veillette, C. Bena, and L. Balents, Phys. Rev. B **69**, 075319 (2004).
- ⁴⁶ A. Kubetzka, M. Bode, O. Pietzsch, and R. Wiesendanger, Phys. Rev. Lett. **88**, 057201 (2002).